Full Waveform Inversion

Source time function inversion and geometrical spreading correction

Thomas Bohlen

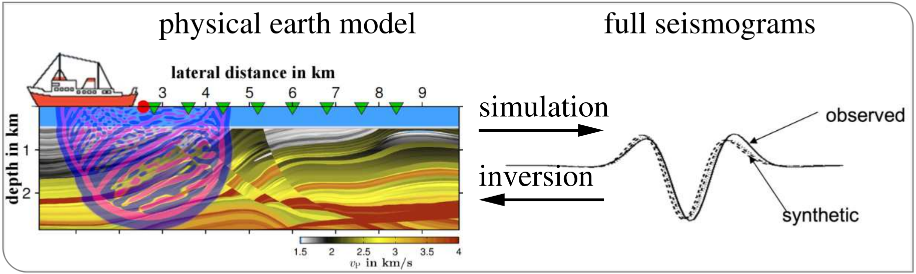

Agenda

1. Source time function inversion

2. Geometrical spreading correction

2.1 Application to surface waves

2.2 Application to reflected body waves

3. Summary

Agenda

1. Source time function inversion

2. Geometrical spreading correction

2.1 Application to surface waves

2.2 Application to reflected body waves

3. Summary

Source time function inversion

Karlsruhe Institute of Technology

The synthetic seismograms of one source at one receiver at position x_r can be calculated with the Green's function of the model m_0 via a convolution:

$$u(x_r, t) = \int_0^T G_{m_0}(x_s, x_r, t - t')s(t')\, dt' \tag{1}$$

A convolution in time domain corresponds to a multiplication in frequency domain:

$$u(x_r, \omega) = G_{m_0}(x_s, x_r, \omega)s(\omega) \tag{2}$$

Source time function inversion

The observed data can be described in the same way, only that the Green's function of the true model and the true source are used.

$$d_{obs}(x_r, \omega) = G_{m_{true}}(x_s, x_r, \omega) s_{true}(\omega) \quad (3)$$

Our goal is to find a linear filter $c(\omega)$ in the frequency domain so that

$$s_{true}(\omega) - c(\omega)s(\omega) = \min \quad (4)$$

The filter $c(\omega)$ is called *source wavelet correction filter*.

Source time function inversion

We make the assumption

$$G := G_{m_0} = G_{m_{true}} \tag{5}$$

Then we can multiply the minimum condition with G, which gives

$$G(s_{true} - cs) = d_{obs} - cu = \min \tag{6}$$

We can thus apply the filter c to the synthetic seismograms u instead of applying it on the synthetic source

Source time function inversion

For minimization, we formulate the difference in (6) as L2-norm:

$$J_s = \sum_{k=1}^{M} \int_w |d_{obs}(x_k, \omega) - c(w)u(x_k, \omega)|^2 \, d\omega + \underbrace{\varepsilon^2 \int_w |c(\omega)|^2 \, d\omega}_{damping} \tag{7}$$

The summation over k considers that we have multiple (M) receivers at the locations x_k.
The second term is a damping term that will assure numerical stability by avoiding a division by zero.
For discrete frequencies $w_l = l\Delta\omega$, $l = 0, \ldots, N-1$, we can write

$$J_s = \left(\sum_{k=1}^{M} \sum_{l=0}^{N-1} |d_{obs}(x_k, \omega_l) - c(\omega_l)u(x_k, \omega_l)|^2 + \varepsilon^2 \sum_{l=0}^{N-1} |c(\omega_l)|^2 \right) \Delta\omega \tag{8}$$

Source time function inversion

We write the filter components $c(\omega_l)$ as sum of real and imaginary part:

$$c(\omega_l) = c_l = c_{l,R} + ic_{l,I} \tag{9}$$

The function J_s is minimized when all partial derivatives are zero, so

$$\frac{\partial J_s}{\partial c_{l,R}} = 0 \quad \text{and} \quad \frac{\partial J_s}{\partial c_{l,I}} = 0 \tag{10}$$

Source time function inversion

If we split also the wavefields d_{obs} and u up into their real and imaginary parts, we can calculate both partial derivatives. The summation of both results gives us the result for the filter components

$$\boxed{c_l = \frac{\sum_{k=1}^{M} u^*(x_k, \omega_l) d_{obs}(x_k, \omega_l)}{\varepsilon^2 + \sum_{k=1}^{M} |u(x_k, \omega_l)|^2}} \tag{11}$$

This filter is called *Wiener-filter* or *water-level deconvolution*.

Source time function inversion

Karlsruhe Institute of Technology

For the application of the source time function inversion in FWI, there are some additional remarks:

- An advantage of this method is that the filter coefficients c_l are resulting from a direct inversion, i.e. only one iteration step is needed
- The filtered signal $c(\omega)s(\omega)$ corresponds approximately to the true source signal
- A stable and causal result for s_{true} indicates a stable convergence
- For the synthetic source s, any signal is possible, e.g. a δ-impulse or a Ricker wavelet
- In FWI, the source time function inversion is applied once per frequency interval
- The same method can be applied to invert receiver-function correction filters

Agenda

2D and 3D Geometrical Spreading

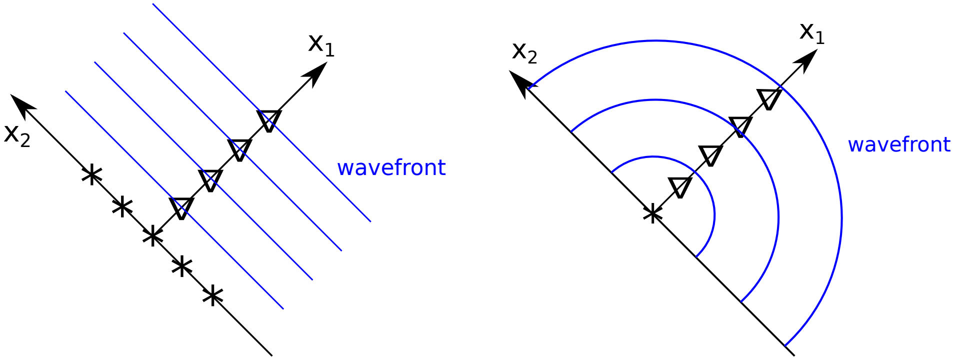

(a) 2D simulation: Line source

(b) 3D field data: Point source

Figure: Description of geometrical spreading in 2D simulation and 3D field data.

Green's functions for acoustic wave equation

Karlsruhe Institute of Technology

Our goal is to find a filter $F(r, k)$ in frequency domain that transforms the 3D data into 2D data assuming a line source. Here, r denotes the distance to the source. In order to find this filter, we consider the acoustic wave equation

$$\left[\frac{\partial^2}{\partial t^2} - c^2(x)\Delta\right] u(x,t) = f(x,t) \tag{12}$$

The Green's function $G(x, x_s, t)$ is the solution of

$$\left[\frac{\partial^2}{\partial t^2} - c^2(x)\Delta\right] G(x, x_s, t) = \delta(x - x_s)\delta t \tag{13}$$

with the source location x_s. In frequency domain, this equation corresponds to

$$\left[k^2 + \Delta\right] \mathcal{G}(x, x_s, \omega) = -4\pi\delta(x - x_s) \tag{14}$$

Green's functions for acoustic wave equation

Assuming a constant velocity c, we obtain the follwing solutions in the far field:

$$\text{3D}: \quad G^{3D}(x, x_s, \omega) = \frac{e^{ikr}}{r} \tag{15}$$

$$\text{2D}: \quad G^{2D}(x, x_s, \omega) = \sqrt{\frac{2\pi}{kr}} e^{ikr} e^{i\pi/4} \tag{16}$$

with $r = ||x - x_s||$. These solutions can be proved by transforming the Laplace operator in equation (14) into spherical (3D) or polar coordinates (2D) and then inserting the Green's functions.

Correction filter

The correction filter F should tranform the 3D data into 2D data, therefore it can be applied on the Green's function, so that $G^{2D} = F(r,k)G^{3D}$ (Forbriger et al. 2014). Thus we have

$$F(r,k) = \frac{G^{2D}}{G^{3D}} = \sqrt{\frac{2\pi r}{k}} e^{i\pi/4} \tag{17}$$

The factor $e^{i\pi/4}$ effects a phase shift of $\frac{\pi}{4}$, and the squared term effects a correction of the amplitudes. With $k = \frac{\omega}{c}$, this can be written as

$$F(r,k) = \sqrt{2rc}\sqrt{\frac{\pi}{\omega}}\, e^{i\pi/4} = \sqrt{2rc}\,\mathrm{FT}\{\sqrt{t^{-1}}\} = F_{amp}\,\mathrm{FT}\{\sqrt{t^{-1}}\}, \tag{18}$$

where $\mathrm{FT}\{\sqrt{t^{-1}}\}$ is the Fourier transform of the function $\sqrt{t^{-1}}$ (Forbriger et al. 2014). We define this now as the phase correction. It is independent of r and easy to implement.

Amplitude correction

The amplitude correction $F_{amp} = \sqrt{2rc}$ depends on the travel distance r. The relation $r = ||x - x_s||$ is only valid for a homogeneous medium, where no reflections can occur. This leads to different practical implementations of the amplitude correction depending on the travel path of the waves. We will here take a look at two different cases (Forbriger et al. 2014)

Amplitude correction in reflection seismic

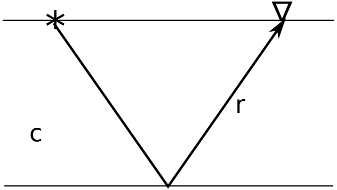

Figure: Travel path of a reflected wave

If reflected waves are recorded, their travel path r is in the beginning unknown and can only be calculated if we know the model velocity. With an average velocity c and the recorded time t, the travel path is $r = ct$. We substitute r in the amplitude correction term to eliminate it, so that

$$F_{amp} = \sqrt{2rc} = c\sqrt{2t} \tag{19}$$

The amplitude correction factor thus is proportional to the square root of the travel time, which makes the correction quite simple. It works only well in smooth models and for not too complex wave paths.

Amplitude correction in shallow seismics

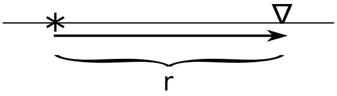

Figure: Travel path of a direct wave

For shallow seismic fields, the waves are travelling nearly on the direct wave, so that the travel path r is equal to the offset and therefore known. We can thus eliminate the unknown velocity c in the amplitude correction factor via $c = \frac{r}{t}$:

$$F_{amp} = \sqrt{2rc} = r\sqrt{\frac{2}{t}} \tag{20}$$

Even if the spreading correction was initially derived for a homogeneous acoustic medium, this correction for shallow surface seismics works surprisingly well also for elastic surface waves (Schäfer et al. 2014).

Agenda

True model

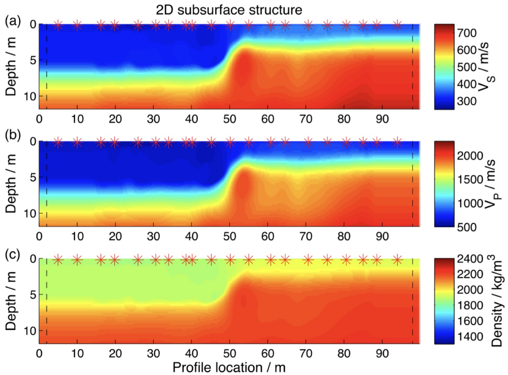

Figure 1. 2-D test structure for 2-D and 3-D modelling as well as for the reconstruction tests. For point-source simulations (3-D) the structure is uniformly extended over 40 m in the third spatial dimension. (a) Displays the *S* velocity, (b) the *P* velocity and (c) the density model. For a better visualization the model is cut off in a depth of 12 m. The FD-grid extends to a depth of 20 m. The absorbing boundary with convolutional perfectly matched layers (CPML) is indicated with black dashed lines. The red stars denote the source locations. The colour bars are chosen to cover this and following figures.

Schäfer et al. (2014)

2D and 3D seismograms

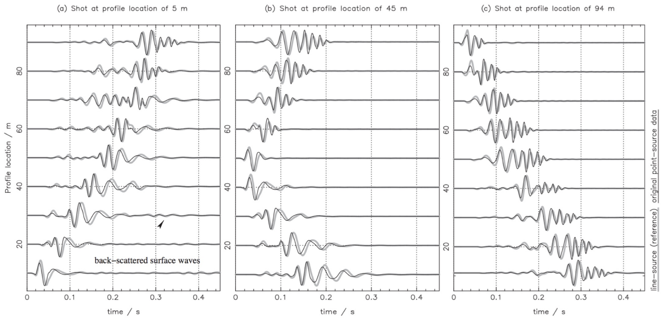

Figure 2. Comparison of line-source seismograms and point-source seismograms (vertical particle velocity) for the true model in Fig. 1; only every 10th trace is displayed. Seismogram (a) shows a shot at profile location of 5 m (very left part of the model), seismogram (b) of 45 m (middle of the model) and seismogram (c) of 94 m (very right part of the model). The seismograms are trace normalized otherwise comparison would not be possible due to different decay of amplitudes.

Schäfer et al. (2014)

Amplitude versus offset

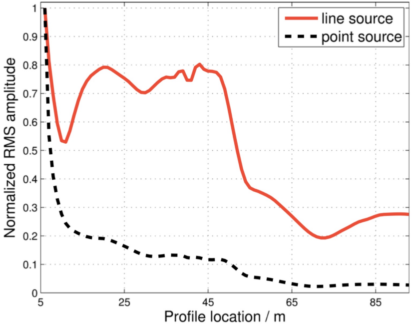

Figure 3. Comparison of amplitude-decay with offset of waves excited by a line source (red line) and a point source (dashed black line) for a shot at profile location of 5 m (vertical component). The rms amplitude is normalized to nearest offset trace.

Schäfer et al. (2014)

Geometrical spreading correction

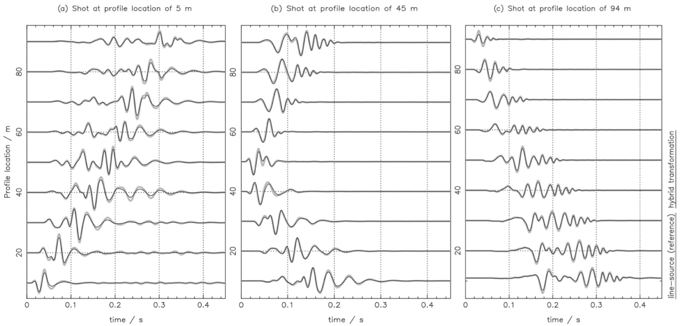

Figure 6. Result of *hybrid* transformation for the radial component: comparison of line-source seismograms and transformed point-source seismograms (radial particle velocity) with the *hybrid* transformation for the true model in Fig. 1; only every 10th trace is displayed. Seismogram (a) shows a shot at profile location of 5 m (very left-hand part of the model), seismogram (b) of 45 m (middle of the model) and seismogram (c) of 94 m (very right part of the model). The seismograms are not trace normalized but scaled by an offset dependent factor $(r/1\,\mathrm{m})^{0.3}$.

Schäfer et al. (2014)

FWI of line-source seismograms

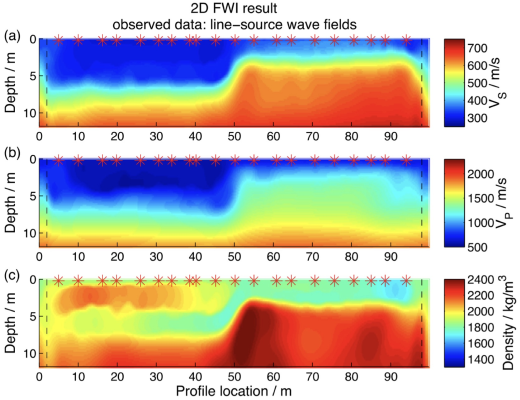

Figure 9. 2-D FWI result using perfect line-source wavefields as observed data. The absorbing boundary with convolutional perfectly matched layers (CPML) is indicated with black dashed lines. (a) Displays the *S* velocity, (b) the *P* velocity and (c) the density model.

Schäfer et al. (2014)

FWI of point-source seismograms

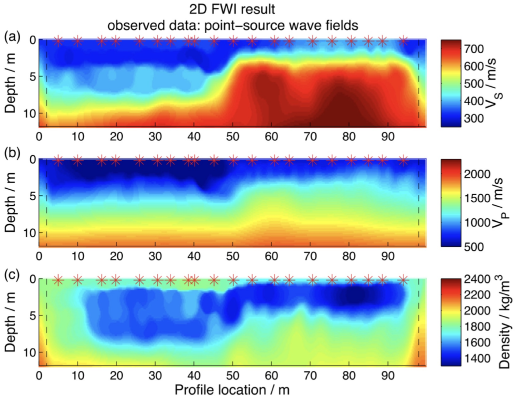

Figure 10. 2-D FWI result using point-source wavefields as observed data. The absorbing boundary with convolutional perfectly matched layers (CPML) is indicated with black dashed lines. (a) displays the *S* velocity, (b) the *P* velocity and (c) the density model.

Schäfer et al. (2014)

FWI of corrected point-source seismograms

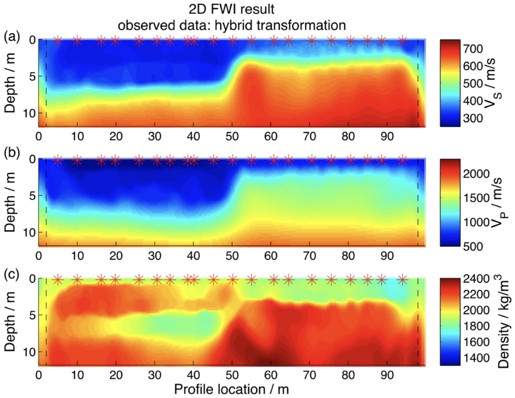

Figure 11. 2-D FWI result using transformed point-source seismograms with *hybrid* transformation as observed data. The absorbing boundary with convolutional perfectly matched layers (CPML) is indicated with black dashed lines. (a) displays the *S* velocity, (b) the *P* velocity and (c) the density model.

Schäfer et al. (2014)

Comparison of FWI results (V_s)

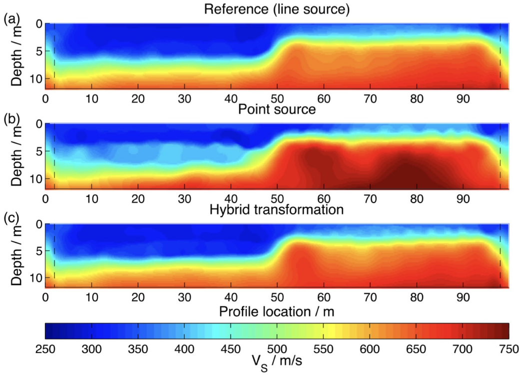

Figure 12. Comparison of 2-D FWI result (*S*-velocity model only) using perfect line-source and transformed point-source wavefields as observed data. (a) Displays the reconstructed *S*-velocity model using line-source seismograms, (b) original point-source seismograms and (c) transformed point-source seismograms with *hybrid* transformation. The absorbing boundary with convolutional perfectly matched layers (CPML) is indicated with black dashed lines.

Schäfer et al. (2014)

Agenda

Simple Marmousi model

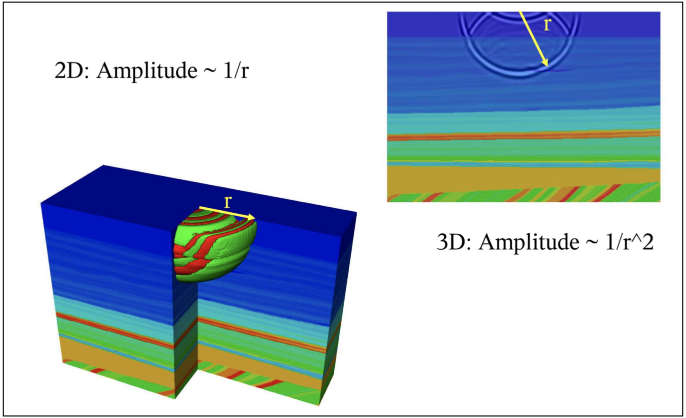

Köhn (2011)

Simple Marmousi model

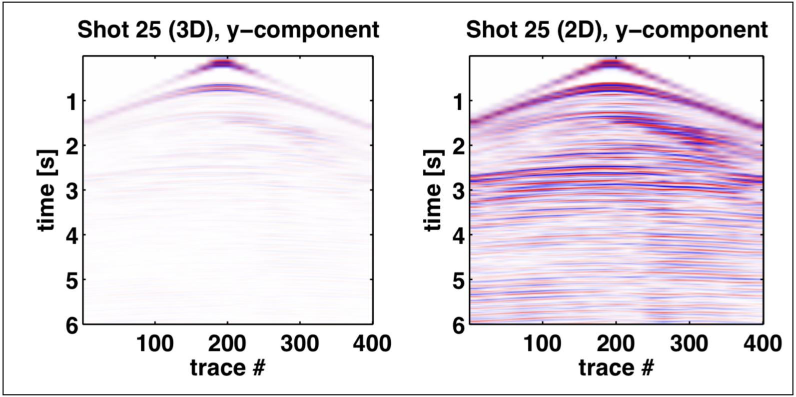

Köhn (2011)

Simple Marmousi model

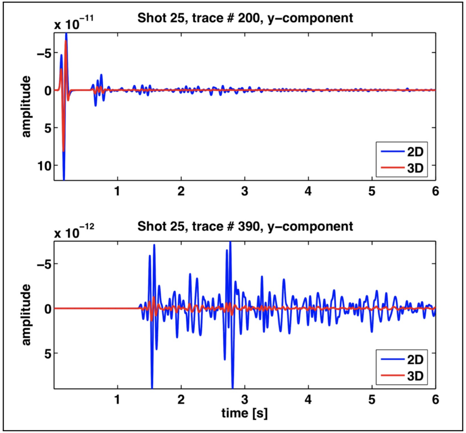

Köhn (2011)

Simple Marmousi model

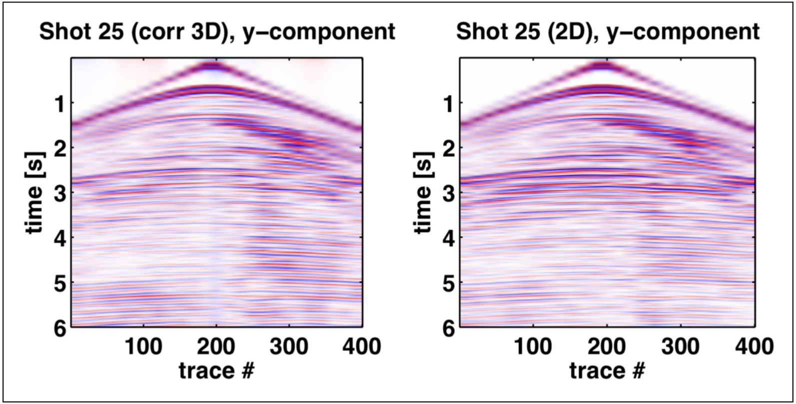

Köhn (2011)

Simple Marmousi model

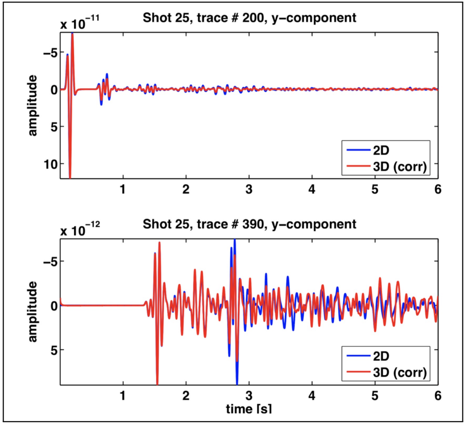

Köhn (2011)

Simple Marmousi model

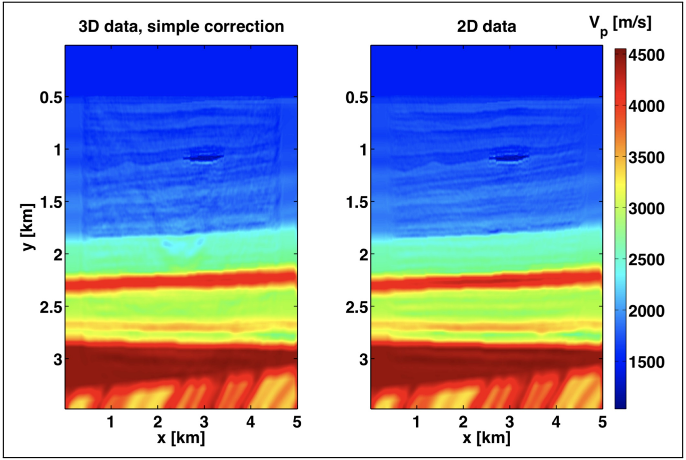

Köhn (2011)

Simple Marmousi model

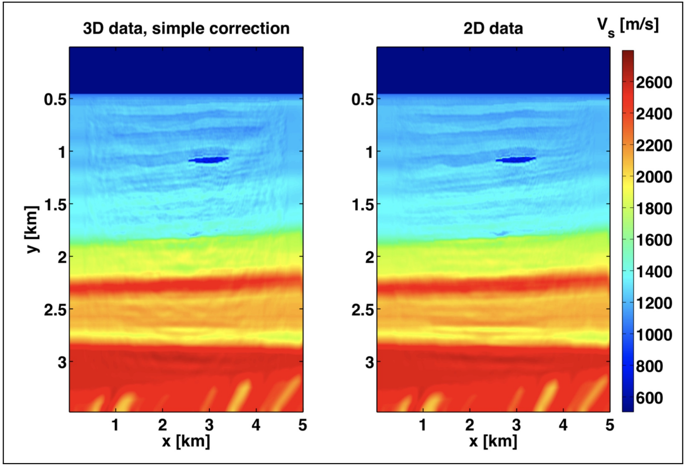

Köhn (2011)

Simple Marmousi model

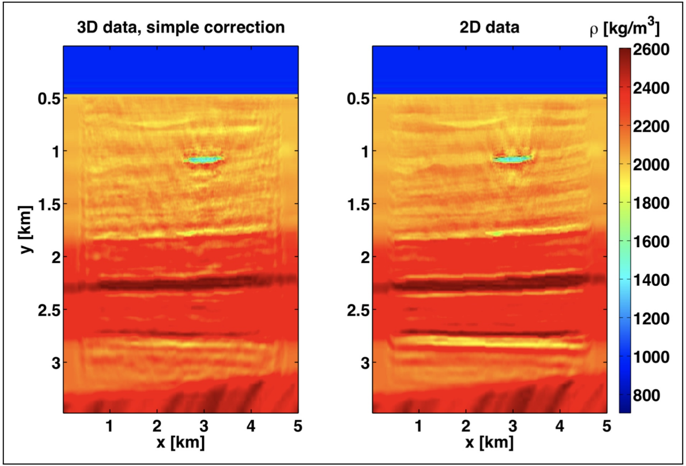

Köhn (2011)

Complex Marmousi model

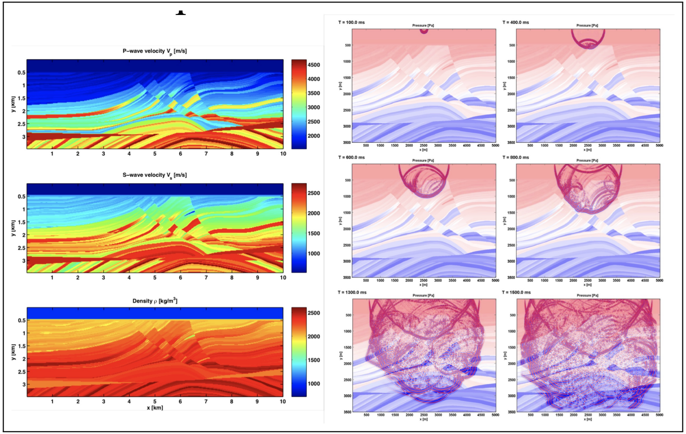

Köhn (2011)

Complex Marmousi model

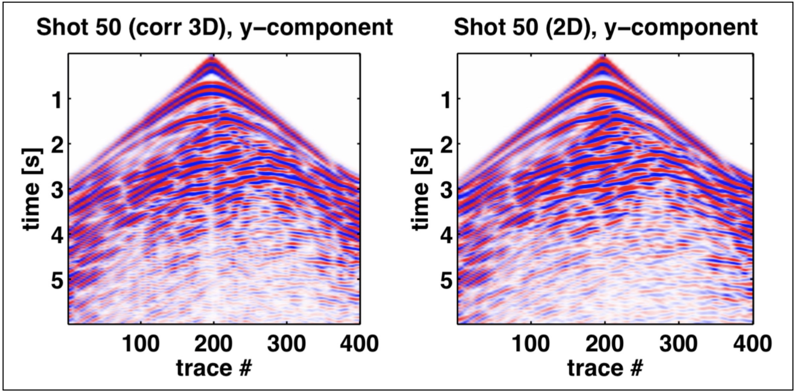

Köhn (2011)

Complex Marmousi model

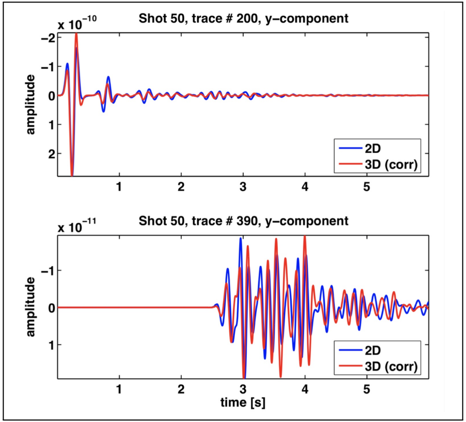

Köhn (2011)

Complex Marmousi model

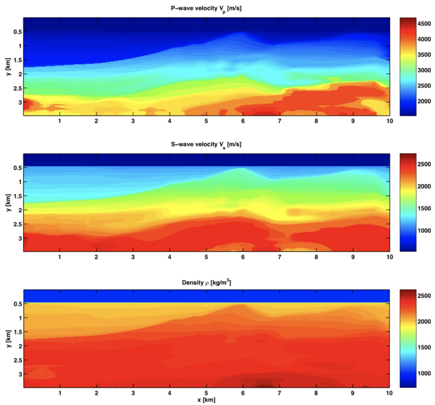

Figure 6.4: Starting models for the Marmousi-II model.

Köhn (2011)

Complex Marmousi model

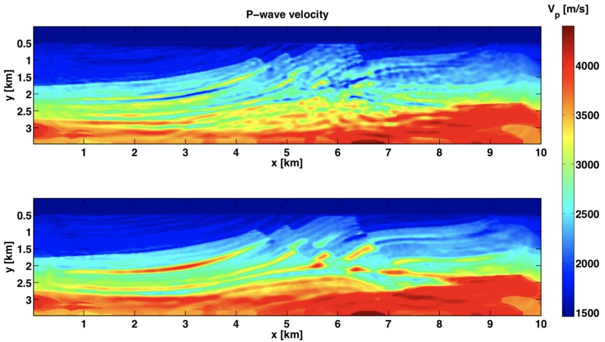

Figure 11.9: FWT results for complex Marmousi2 model. The P-wave velocity model V_p estimated by the corrected 3D data (top) is compared with the result of the 2D data inversion (bottom).

Köhn (2011)

Complex Marmousi model

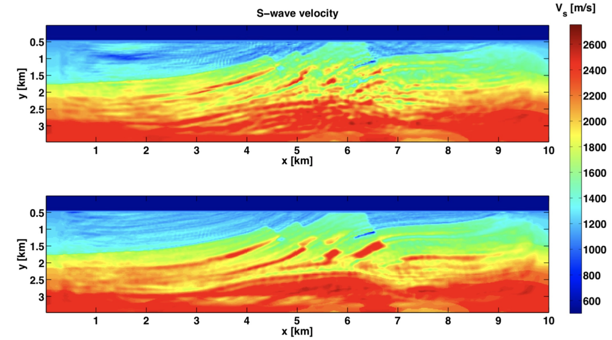

Figure 11.10: FWT results for complex Marmousi2 model. The S-wave velocity model V_s estimated by the corrected 3D data (top) is compared with the result of the 2D data inversion (bottom).

Köhn (2011)

Complex Marmousi model

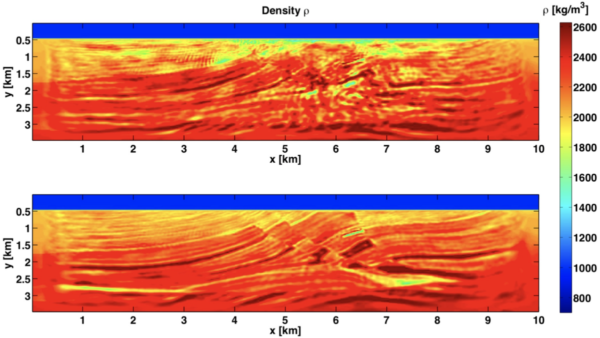

Figure 11.11: FWT results for complex Marmousi2 model. The density model ρ estimated by the corrected 3D data (top) is compared with the result of the 2D data inversion (bottom).

Köhn (2011)

Applications of geometrical spreading corrections

Surface waves

- works surprisingly well for shallow seismic wave fields
- single-trace transformation
- applicable also in case of lateral heterogeneity

Reflected elastic wavefield

- works sufficiently well in case of moderate structural heterogeneity (simple Marmousi model)
- artifacts in FWI reconstructions in case of strong structural heterogeneity (complex Marmousi model)
- no universal solution available

Agenda

Thank you for your attention

Thomas.Bohlen@kit.edu

http://www.gpi.kit.edu/

References

Forbriger, T., Groos, L. & Schäfer, M. (2014), 'Line-source simulation for shallow-seismic data. Part 1: theoretical background.', *Geophysical Journal International* **198**(3), 1387–1404.

Köhn, D. (2011), Time Domain 2D Elastic Full Waveform Tomography, PhD thesis, Kiel University.
URL: *http://macau.uni-kiel.de/receive/dissertation_diss_00006786*

Schäfer, M., Groos, L., Forbriger, T. & Bohlen, T. (2014), 'Line-source simulation for shallow-seismic data. part 2: full-waveform inversion—a synthetic 2-D case study', *Geophysical Journal International* **198**(3), 1405–1418.
URL: *http://gji.oxfordjournals.org/content/198/3/1405.abstract*